Blue–green–red luminescence from $CeCl_3$- and $MnCl_2$-doped hafnium oxide layers prepared by ultrasonic spray pyrolysis

2008 J. Phys.: Condens. Matter 20 395205

(http://iopscience.iop.org/0953-8984/20/39/395205)

J. Phys.: Condens. Matter **20** (2008) 395205 (7pp) doi:10.1088/0953-8984/20/39/395205

Blue–green–red luminescence from $CeCl_3$- and $MnCl_2$-doped hafnium oxide layers prepared by ultrasonic spray pyrolysis

R Martínez-Martínez[1], M García[2], A Speghini[3], M Bettinelli[4], C Falcony[5] and U Caldiño[1]

[1] Departamento de Física, Universidad Autónoma Metropolitana-Iztapalapa, PO Box 55-534, 09340 México, DF, Mexico
[2] Instituto de Investigaciones en Materiales, UNAM, AP 70-360 Coyoacán, 04510 México, DF, Mexico
[3] DiSTeMeV, Università di Verona, and INSTM, UdR Verona, Via della Pieve 70, I-37029 San Floriano, Verona, Italy
[4] Dipartimento Scientifico e Tecnologico, Università di Verona, and INSTM, UdR Verona, Strada Le Grazie 15, I-37314 Verona, Italy
[5] Centro de Investigaciones y Estudios Avanzados del IPN, Departamento de Física, PO Box 14-7400, 7000 México, DF, Mexico

E-mail: cald@xanum.uam.mx

Received 5 April 2008, in final form 31 July 2008
Published 1 September 2008
Online at stacks.iop.org/JPhysCM/20/395205

Abstract

Hafnium oxide films doped with $CeCl_3$ and/or $MnCl_2$, and deposited at 300 °C by an ultrasonic spray pyrolysis process, were characterized using x-ray diffraction (XRD), energy-dispersive spectroscopy and photoluminescence. The XRD results revealed that the films are predominantly amorphous. The weak green–red emission of Mn^{2+} is enhanced through an efficient energy transfer from Ce^{3+} to Mn^{2+} ions. Spectroscopic data revealed that the energy transfer is nonradiative in nature and it could occur in Ce^{3+} and Mn^{2+} clusters through a short-range interaction mechanism. The efficiency of this transfer increases with the Mn^{2+} ion concentration, so that an efficiency of about 78% is attained for a 5 at.% of $MnCl_2$ concentration, which makes these films interesting phosphors for the design of luminescent layers with blue, green and red emissions.

1. Introduction

Many investigations of the luminescent properties of rare-earth (RE) or transition-metal-ion-doped compounds have been performed during the last decades. These investigations are very important from the standpoint of the development of efficient luminescent materials applied as phosphors used in next-generation displays. Such displays require materials capable of emitting more efficiently the three primary colors [1]. In addition, the growing flat panel display market during the last decade has brought about a resurgence of interest in phosphor materials as well as their synthesis and characterization.

Hafnium oxide (HfO_2) has attracted considerable attention due to its excellent chemical and physical properties, such as its high dielectric constant and insulating characteristics [2]. The application of this oxide is, then, as a dielectric material with relatively high dielectric constant, high refractive index and wide bandgap. These properties make it a good candidate for applications in the field of optical coatings and metal-oxide semiconductor devices of the next generation [3]. However, systematic studies on the luminescent properties of optically active ions doped in hafnium oxide are scarce. Only a few studies on Tb^{3+}- [4], Eu^{3+}- [4, 5], Er^{3+}- [6], Ce^{3+}- [7] and Mn^{2+}- [8] doped HfO_2 have been recently reported.

The search for more efficient blue-emitting phosphors has found some Ce^{3+}-containing materials, such as Ce^{3+}-doped AlO_2 thin films [9]. Moreover, Ce^{3+}-activated materials have attracted renewed interest due to their favorable spectroscopic properties, and the fact that the Ce^{3+} ion acts as a good sensitizer, transferring a part of its energy to activator ions such as Tb^{3+} [10], Eu^{2+} [11, 12] and Mn^{2+} [12, 13]. The Ce^{3+} ion in solids shows efficient broad band luminescence due to its 4f–5d parity-allowed electric dipole transition. This ion has high oscillator strength and a much larger Stokes shift than the f–f transitions of other RE^{3+} ions, due to the extended radial wavefunctions of the 5d state [14].

The Mn^{2+} ions with configuration $3d^5$ are important activators in many commercial luminescent materials [15]. The Mn^{2+} ion in solids can generate a broad emission band from the green to red, depending on the host lattice, due to its transition $^4T_1(G) \rightarrow {}^6A_1(G)$ [16–18].

Luminescent materials incorporating more than one center can present energy transfer phenomena from one center to another [19]. In particular, it is well known that Ce^{3+} ions are excellent sensitizers of excitation energy and Mn^{2+} ions act as efficient activators. Both ions have been used as dopants in photoluminescent materials involving energy transfer [20, 21] in the quest for efficient blue- and red-emitting materials.

In this work we have performed an exhaustive analysis of the blue, green and red photoluminescence of HfO_2:Ce^{3+}:Mn^{2+} films synthesized by the ultrasonic spray pyrolysis technique. This technique has proved to be very efficient and an interesting alternative to synthesize luminescent films. Thus, the spray pyrolysis deposition process has advantages such as low cost, a high deposition rate, ease of operation and capacity to deposit films on large areas [22].

To our knowledge no work has been reported on the optical spectroscopy of HfO_2 films doubly doped with Ce^{3+} and Mn^{2+} ions.

2. Experimental details

HfO_2:Ce^{3+}, HfO_2:Mn^{2+} and HfO_2:Ce^{3+}:Mn^{2+} films (deposited by ultrasonic spray pyrolysis) were obtained from an aqueous solution containing $HfOCl_2{\cdot}8H_2O$, $CeCl_3{\cdot}7H_2O$ and/or $MnCl_2{\cdot}4H_2O$ (Aldrich Chemical Co). The last two solutions were added as doping materials. The exact preparation of the spray solution is described elsewhere [8]. The $CeCl_3$ concentration in the spraying solution was fixed at around 3 at.%, varying only the $MnCl_2$ concentration (1, 3 and 5 at.%). Hereafter, the cerium-and/or manganese-doped HfO_2 films: HfO_2:$CeCl_3$ (3 at.%), HfO_2:$CeCl_3$ (3 at.%):$MnCl_2$ (1 at.%), HfO_2:$CeCl_3$(3 at.%):$MnCl_2$ (3 at.%), HfO_2:$CeCl_3$(3 at.%):$MnCl_2$ (5 at.%) and HfO_2:$MnCl_2$ (5 at.%) will be referred to as Ce3, Ce3Mn1, Ce3Mn3, Ce3Mn5 and Mn5, respectively. The molar ratio of the spraying solution was 0.07. The films were sprayed onto Corning 7059 glass slides used as substrates. The substrate temperature during deposition was set at 300 °C. The carrier gas flow (filtered air) was 12 l min^{-1}. The deposition time was adjusted (5–6 min) in order to obtain similar thicknesses for all the films studied.

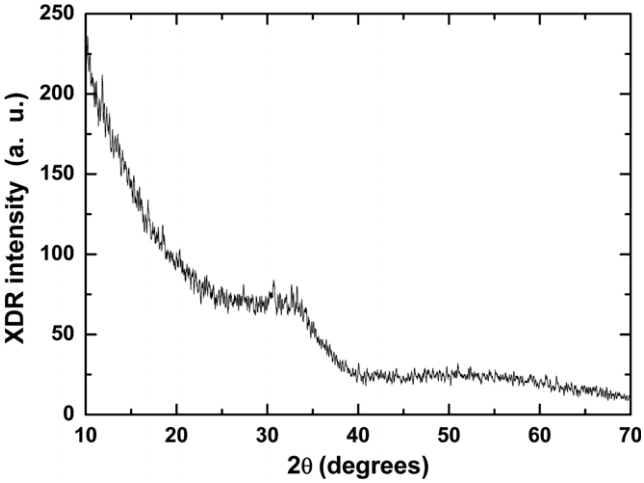

Figure 1. XRD patterns for the Ce3, Ce3Mn1, Ce3Mn3, Ce3Mn5 and Mn5 films grown at 300 °C.

The thicknesses were approximately 5 ± 0.03 μm as measured by a Sloan Dektak IIA profilometer.

The structure of the sprayed films was characterized by means of x-ray diffraction (XRD) using a Siemens D-5000 diffractometer at 1.5406 Å (Cu Kα). This was operated at 30 keV. The chemical composition of the films was measured by means of energy-dispersive spectroscopy (EDS) using an Oxford Pentafet equipped with a beryllium window and x-ray detector integrated in a Leica-Cambridge electron microscope model Stereoscan 440. The photoluminescence measurements were carried out using a Perkin-Elmer LS50B fluorescence spectrophotometer. The decay curves of the Ce^{3+} and Mn^{2+} emissions were recorded by excitation at 355 nm by means of a pulsed Nd:YAG laser. A fiber optic probe was employed to collect the emission. The emitted light was dispersed by means of a half-meter monochromator equipped with a 150 lines mm^{-1} grating, and finally detected by a GaAs photomultiplier. The signal detected by the photomultiplier was then averaged and recorded by a digital oscilloscope. The short decay times of the Ce^{3+} emission were obtained from the decay curves using a deconvolution procedure, which takes into account the shape and duration (about 8–10 ns) of the excitation pulse. The decay curve of the Mn^{2+} emission recorded with 410 nm excitation was obtained with the Perkin-Elmer LS50B fluorescence spectrophotometer operated in the mode of phosphorescence.

All the measurements were carried out at room temperature.

3. Results

3.1. XRD and EDS measurements

XRD patterns are independent of the introduction of dopants ($CeCl_3$ and/or $MnCl_2$). The XRD patterns displayed by the Ce3, Ce3Mn1, Ce3Mn3, Ce3Mn5 and Mn5 films exhibited very poor crystallinity (figure 1), so that they can be considered as predominantly amorphous.

Table 1. Atomic per cent content of oxygen, hafnium, cerium, manganese and chlorine in the undoped and doped films as measured by EDS.

Film	Oxygen (at.%)	Hafnium (at.%)	Cerium (at.%)	Manganese (at.%)	Chlorine (at.%)
Undoped	64.0	31.9	—	—	4.1
Ce3	54.9	34.6	1.9	—	8.6
Ce3Mn1	54.5	32.9	2.0	0.9	9.7
Ce3Mn3	52.9	32.9	1.8	1.6	10.8
Ce3Mn5	54.7	32.2	1.6	2.0	9.5
Mn5	55.4	33.4	—	2.5	8.7

The relative atomic percentages of oxygen, hafnium, cerium, manganese and chlorine in the doped HfO_2 films (determined by EDS) as a function of the $CeCl_3$ and/or $MnCl_2$ contents in the spraying solution are listed in table 1. In this table the relative atomic percentages of oxygen, hafnium and chlorine for the undoped HfO_2 sample are also displayed. It can be seen that, in the undoped sample, the hafnium (31.9 at.%), oxygen (64.0 at.%) and chlorine (4.1 at.%) contents are consistent with a stoichiometric HfO_2 film. In the HfO_2 films doped with Ce and/or Mn by adding $CeCl_3$ and/or $MnCl_2$ to the spraying solution, the Hf content remains close to 33 at.%, but the O content is about 54 at.%, while the Cl content is around 9 at.%. If the trivalent cerium and divalent manganese ions substitute for hafnium cation ions, the incorporated chlorine ions could act as charge compensators to preserve electrical neutrality [7]. Therefore, the hafnium ions might remain with their 4+ charge.

3.2. Photoluminescence

Figure 2 portrays emission spectra of HfO_2 singly doped with Ce^{3+} ions and codoped with Mn^{2+} ions after 290 nm excitation within the $Ce^{3+}4f \rightarrow 5d$ absorption transition. All these spectra have been recorded at the same experimental conditions for comparison. They consist of a broad band in the blue region centered at around 400 nm, which is associated with the transition from the $5d^1$ configuration to the $4f^1$ one of Ce^{3+} ions. The asymmetric spectral feature of the Ce^{3+} emission does not present the expected doublet associated with the transition from the excited state to the $^2F_{5/2}$ and $^2F_{7/2}$ levels of the ground state, as reported in, for example, Ce^{3+}-doped CaF_2 crystals [11–13]. This lack of spectral structure is attributed to a strong inhomogeneous broadening, due to the disordered nature of the hafnium oxide host. The outstanding feature in the emission spectra of figure 2 is that the addition of Mn^{2+} ions in the Ce^{3+}-doped film causes a decrease of the overall cerium emission. This fact provides evidence that energy transfer from Ce^{3+} to Mn^{2+} ions occurs by means of a nonradiative process.

A broad emission band located in the green–red region is observed by codoping the HfO_2:$CeCl_2$ film with $MnCl_2$. Therefore, this emission band can be attributed to the $^4T_1(G) \rightarrow {}^6A_1(S)$ transition of Mn^{2+} ions. Figure 3 shows emission spectra of the three doubly doped films under investigation, which were recorded with a delay of 0.1 ms after the 290 nm excitation pulse, so that the Mn^{2+} emission is well resolved from the fast Ce^{3+} blue emission. The Ce3Mn1 film displays a broad emission band peaking at about 602 nm in the yellow–red region. A pronounced shoulder located

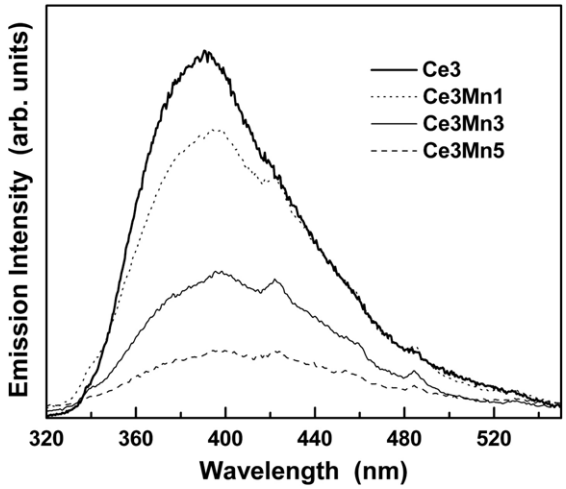

Figure 2. Emission spectra of HfO_2 singly doped with Ce^{3+} ions and codoped with Mn^{2+} ions after 290 nm excitation. All the spectra have been obtained in the same experimental conditions.

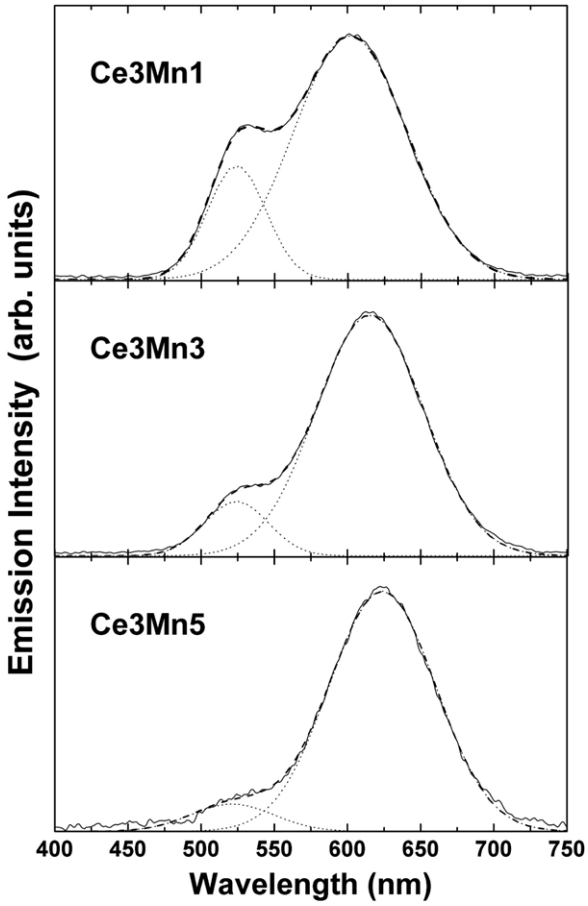

Figure 3. Emission spectra recorded with a 0.1 ms delay time of the Ce3Mn1, Ce3Mn3 and Ce3Mn5 films excited at 290 nm. The spectra have been fitted by two Gaussian bands (dotted line), so that the solid line corresponds to the emission band and the dashed line to the analytical fit.

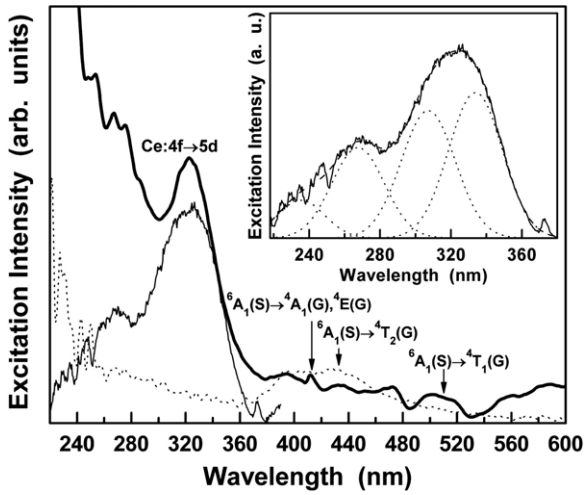

Figure 4. Excitation spectra of the Ce3 (solid thin line), Ce3Mn5 (solid thick line) and Mn5 (dotted line) films. The spectra were monitored at 440 nm for the Ce3 film and at 620 nm (with a 0.1 ms delay time) for the films containing Mn^{2+}. The inset shows the Ce3 excitation spectrum fitted by four Gaussian bands (dotted line).

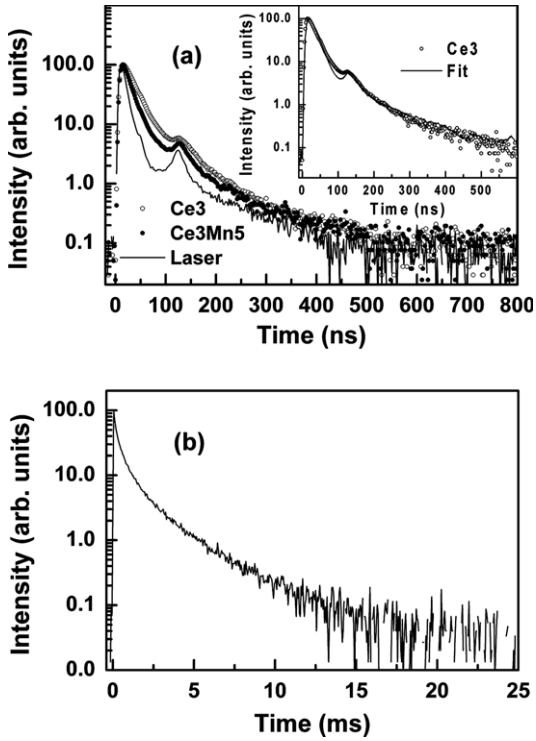

Figure 5. (a) Decay curves of the Ce^{3+} emission, $\lambda_{ex} = 355$ nm and $\lambda_{em} = 440$ nm, for the Ce3 and Ce3Mn5 films. The inset displays the experimental and fitted decay curves of the Ce^{3+} emission for the Ce3 film. (b) Decay curve of the Mn^{2+} emission, $\lambda_{ex} = 355$ nm and $\lambda_{em} = 620$ nm, for the Ce3Mn5 film.

at 532 nm, in the green region, can also be observed. The emission spectra for higher manganese concentration films (3 at.% and 5 at.%) show a wavelength redshift, such that the peak position is shifted from 602 to 615 nm, and from 615 to 624 nm (in the red region), on passing from 1 to 3 at.%, and from 3 to 5 at.% of $MnCl_2$, respectively. On the other hand, the green emission band tends to disappear on increasing the manganese concentration. Thus, the emission spectra in figure 3 are well fitted by two Gaussian bands associated with the green and red Mn^{2+} emissions. This behavior of the Mn^{2+} emission band reveals that, in the films under investigation, the Mn^{2+} ion can be located in different environments or coordination numbers. Taking into account that the green and red Mn^{2+} emissions have been usually interpreted in terms of a tetrahedral and octahedral coordination, respectively, then low Mn^{2+} concentration might lead to a tetrahedral coordination, producing a green emission, whereas at high concentrations the Mn^{2+} ion might be characterized by an octahedral coordination, generating a red emission [23].

Excitation spectra of the Ce3, Ce3Mn5 and Mn5 films are displayed in figure 4. The excitation spectrum of the film containing only Ce^{3+} ions was monitored at 440 nm, inside their emission band terminating on the $^2F_{5/2}$ and $^2F_{7/2}$ ground levels. It consists of a broad band extending from 220 to 380 nm, which is well fitted by four Gaussian bands associated with a partial lifting of the degeneracy of the cerium 5d orbitals, see the inset of figure 4. The excitation spectra of the films containing manganese were monitored at 620 nm. In the 380–540 nm region these spectra display several broad bands, which can be associated with the $^6A_1(S) \rightarrow {}^4A_1$, $^4E(G)$, $^6A_1(S) \rightarrow {}^4T_2(G)$ and $^6A_1(S) \rightarrow {}^4T_1(G)$ absorption transitions of Mn^{2+}. A broad band at around 322 nm is observed in the excitation spectrum taken at $\lambda_{em} = 620$ nm for the Ce3Mn5 film, which is similar to that observed in the excitation spectrum of the Ce3 cerium singly doped film, and therefore it must be associated with $Ce^{3+}4f \rightarrow 5d$ absorptions. The presence of this Ce^{3+} band in the excitation spectrum monitored within the Mn^{2+} emission (620 nm) indicates that Mn^{2+} ions can be excited through Ce^{3+} ions by means of an energy transfer process.

3.3. Lifetime measurements

Decay time measurements performed on the Ce^{3+} emission in the Ce3 and Ce3Mn5 films were carried out monitoring the emission at 440 nm after 355 nm laser pulsed excitation within the Ce^{3+} $4f \rightarrow 5d$ absorption band. The Ce^{3+} emission decay curves for the Ce3 and Ce3Mn5 films are displayed in figure 5(a).

In the absence of Mn^{2+} ions the decay time value obtained for the Ce^{3+} emission, once deconvoluted from the Nd:YAG laser excitation pulse profile, resulted to be around 14 ns. This value was found to be independent of the emission wavelength selected for the decay recording. A comparison between the Ce^{3+} emission decay curve and the best one obtained from the fitting procedure is displayed in the inset of figure 5(a).

In the presence of Mn^{2+} the decay curve of the Ce^{3+} emission is remarkably non-exponential due presumably to the $Ce^{3+} \rightarrow Mn^{2+}$ energy transfer process. The decay time value obtained for the Ce^{3+} emission in Ce3Mn5, once deconvoluted from the laser excitation pulse profile, resulted to be around 8 ns. It is worth noting that a shortening of the Ce^{3+} decay time for the Ce3Mn5 sample, with respect to the Ce3 one, can be shown from an inspection of the profiles of the emission decay curves, see figure 5(a). In fact, the emission decay is steeper

for the Ce3Mn5 sample than for the Ce3 one. Considering that the laser excitation pulse has a temporal width of about 8–10 ns, see figure 5(a), then we are at the lower limit of the temporal resolution of the exciting system. Therefore, the decay time of the Ce^{3+} emission in the presence of Mn^{2+} might well be shorter than 8 ns, taking into account that it is not possible to obtain decay times smaller than 8 ns with the present experimental set-up. Anyway, the increase in the Ce^{3+} emission decay rate on codoping with manganese can be attributed to nonradiative energy transfer from Ce^{3+} to Mn^{2+} ions.

The average decay time τ_{av} for the Mn^{2+} emission was obtained from experimental data through the expression

$$\tau_{av} = \frac{\int t I(t)\,dt}{\int I(t)\,dt}, \tag{1}$$

where $I(t)$ is the emission intensity at time t. Decay time measurements on the Mn^{2+} emission at 620 nm in the Ce3Mn5 film yield the same value for τ_{av} (1.5 ± 0.1 ms) when the Mn^{2+} is excited via Ce^{3+} ions at 355 nm, see figure 5(b), or directly excited at 410 nm, as expected from the absence of a $Ce^{3+} \leftarrow Mn^{2+}$ back energy transfer process.

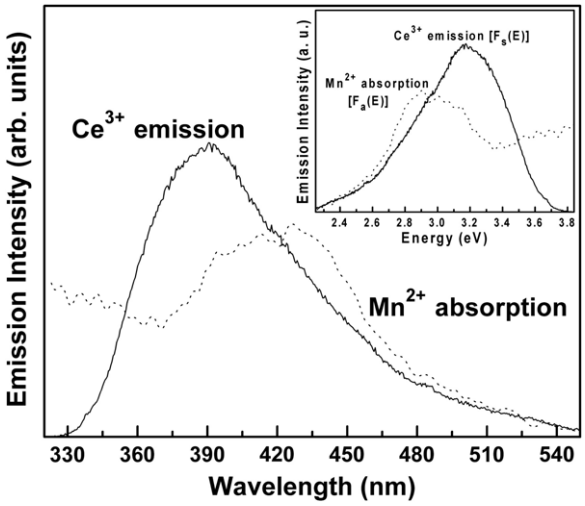

Figure 6. Overlap region between the Ce^{3+} emission (solid line) and Mn^{2+} absorption (dotted line). The inset shows the normalized lineshape functions. The Mn^{2+} absorption spectrum in the overlap region was taken from the Mn5 film excitation spectrum displayed in figure 4.

4. Discussion

The energy transfer from Ce^{3+} to Mn^{2+} ions in the doubly doped films is revealed by:

(i) the presence of $Ce^{3+}4f \rightarrow 5d$ absorption bands in the excitation spectrum of the Mn^{2+} emission, and
(ii) the increase in the Ce^{3+} emission decay rate.

Besides, the transfer process is expected to be resonant considering that the cerium emission overlaps the Mn^{2+} $^6A_1(S) \rightarrow {}^4A_1(G)$, $^4E(G)$, $^6A_1(S) \rightarrow {}^4T_2(G)$ and $^6A_1(S) \rightarrow {}^4T_1(G)$ absorption (excitation) transitions, as can be appreciated from the spectra displayed in figure 6.

The very short decay time measured for the Ce^{3+} emission reveals that the $5d \rightarrow 4f$ transition is electric-dipole-allowed, whereas the long decay time measured for the Mn^{2+} emission reflects the parity- and spin-forbidden character of the $^4T_1(G) \rightarrow {}^6A_1(S)$ transition. Hence, it seems reasonable to assume that the $Ce^{3+} \rightarrow Mn^{2+}$ energy transfer could occur through an electric dipole–quadrupole (d–q) interaction mechanism [19]. Taking into account this assumption, the transfer rate W_{sa}^{dq} for an electric d–q interaction between sensitizer (Ce^{3+}) and activator (Mn^{2+}) ions is given by [24]

$$W_{sa}^{dq} = \frac{3\hbar^4 c^4 f_q \lambda_s^2 Q_a}{4\pi n^4 \tau_s^o f_d R_{sa}^8}\Omega, \tag{2}$$

where $\Omega = \int [F_s(E)F_a(E)/E^4]\,dE$ is the spectral overlap integral between the normalized lineshape functions of the sensitizer emission $F_s(E)$ and activator absorption $F_a(E)$, E being the transfer energy, Q_a is the integrated absorption coefficient of Mn^{2+} ions, f_q and f_d are the oscillator strengths of the Mn^{2+} ion electric quadrupole and dipole transitions, respectively, R_{sa} is the interaction distance between the Ce^{3+} and Mn^{2+} ions involved in the transfer and τ_s^o is the Ce^{3+} ion intrinsic lifetime in the absence of energy transfer. The remaining symbols in equation (2) have their usual meaning. The overlap integral was calculated using the normalized lineshape functions of the cerium emission $F_s(E)$ and manganese absorption $F_a(E)$ in the overlap region (shown in the inset of figure 6). The overlap integral resulted in being 8.8×10^{-3} eV^{-5}. The optical absorption spectrum of Mn^{2+} ions in the overlap region with the Ce^{3+} emission was hardly detectable because of the very weak intensity of their forbidden 3d–3d transitions. Therefore, the function $F_a(E)$ was obtained from the excitation spectrum of the 620 nm emission recorded for the Mn5 film (figure 4), and in equation (2) the Q_a integrated absorption coefficient of Mn^{2+} was estimated using the relationship derived by Blasse, $Q_a = 4.8 \times 10^{-20}$ eV $m^2 \cdot f_d$ [25]. The oscillator strengths of the Mn^{2+} ion, f_q and f_d, are usually considered of order 10^{-10} and 10^{-7}, respectively [26–28].

Let us now estimate the R_{sa}^o critical interaction distance between Ce^{3+} and Mn^{2+} ions for energy transfer to verify if the $Ce^{3+} \rightarrow Mn^{2+}$ transfer arises from randomly distributed ions. Assuming an electrical d–q interaction mechanism, R_{sa}^o can be estimated from equation (2) considering that it is the one for which the probability of transfer equals the probability of radiative emission of the sensitizer ($W_{sa}^{dq}\tau_s^o = 1$). Using the values estimated for Q_a and Ω it is found that $R_{sa}^o = 7.9$Å. We can verify if this critical interaction distance results from an ion random distribution or not. Assuming that there is one ion at the center of a sphere of radius R, then

$$N\frac{4\pi R^3}{3} = 1, \tag{3}$$

where N is the total concentration of Ce^{3+} and Mn^{2+} ions cm^{-3}. Considering that the shorter distance between two randomly

Table 2. W_{sa} rates and η efficiencies of the $Ce^{3+} \rightarrow Mn^{2+}$ energy transfer, and $\bar{R}_{sa}$ average and D_{random} random Ce^{3+}–Mn^{2+} interaction distances in the films Ce3Mn1, Ce3Mn3 and Ce3Mn5.

Film	W_{sa} (s^{-1})	η (%)	$\bar{R}_{sa}$ (Å)	D_{random} (Å)
Ce3Mn1	1.5×10^7	17.0	9.6	9.3
Ce3Mn3	9.3×10^7	56.6	7.6	8.8
Ce3Mn5	2.6×10^8	78.2	6.7	8.6

distributed ions, D_{random}, is equal to $2R$, then from equation (3) [12]

$$D_{random} = 2R = 2\left(\frac{3}{4\pi N}\right)^{1/3}. \quad (4)$$

Thus, the critical interaction distance is smaller than the one (8.6–9.3 Å) obtained assuming a random distribution of Ce^{3+} and Mn^{2+} ions, see table 2. Therefore, it can be concluded that the $Ce^{3+} \rightarrow Mn^{2+}$ energy transfer seems to take place in Ce^{3+}–Mn^{2+} clusters formed in the film, instead of from randomly distributed ions.

The η energy transfer efficiency can help us to evaluate whether the Ce^{3+} ion is a good sensitizer for the Mn^{2+} ion. The η efficiency was then estimated from the emission intensities of the Ce^{3+} sensitizer in the presence (I_s) and absence (I_s^o) of the Mn^{2+} activator, i.e. [10]

$$\eta = 1 - \frac{I_s}{I_s^o}. \quad (5)$$

Thus, the efficiency of energy transfer from Ce^{3+} to Mn^{2+} ions, using equation (5) and the cerium emission spectra shown in figure 2, was found to increase with the Mn^{2+} concentration from around 17% (Ce3Mn1 film) up to around 78% (Ce3Mn5 film), see figure 7 and table 2.

The efficiency of energy transfer can also be expressed in terms of the W_{sa} transfer rate and the τ_s^o sensitizer intrinsic lifetime in the absence of energy transfer [20]:

$$\eta = \frac{W_{sa}\tau_s^o}{1 + W_{sa}\tau_s^o}. \quad (6)$$

So the experimental energy transfer rate can be estimated from equation (6):

$$W_{sa} = \frac{\eta}{(1-\eta)\tau_s^o}. \quad (7)$$

Using the data obtained for η and the value of the Ce^{3+} decay time in the absence of Mn^{2+} for τ_s^o, the $Ce^{3+} \rightarrow Mn^{2+}$ energy transfer rate was found to increase from 1.5×10^7 s^{-1} in the Ce3Mn1 film to 2.6×10^8 s^{-1} in the Ce3Mn5 film (see table 2). A transfer rate in the Ce3Mn1 film smaller than the Ce^{3+} intrinsic decay rate ($1/\tau_s^o = 7.1 \times 10^7$ s^{-1}) is a consequence of its low energy transfer efficiency of less than 50%.

The $\bar{R}_{sa}$ average interaction distance between the Ce^{3+} and Mn^{2+} ions involved in the energy transfer for each of the films, assuming an electric d–q interaction mechanism, was then estimated from equation (2) using the corresponding W_{sa} experimental value estimated from equation (7). These

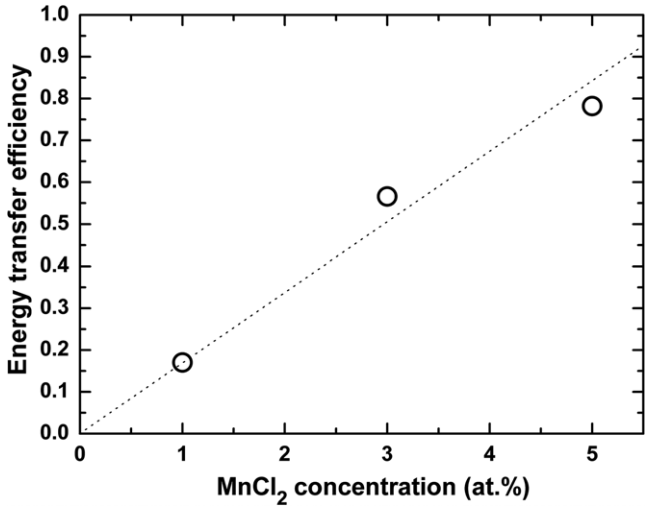

Figure 7. $Ce^{3+} \rightarrow Mn^{2+}$ energy transfer efficiency as a function of manganese concentration obtained from spectral data (figure 2) and equation (5). The dotted line is drawn to guide the eyes.

distances are displayed in table 2. As expected, the Ce^{3+}–Mn^{2+} interaction distance is shortened when the Mn^{2+} content increases. This fact suggests, hence, that in the Ce^{3+}–Mn^{2+} clusters the sensitizer ions tend to be closer to the activator ions as the Mn^{2+} concentration increases. Inspection of table 2 also shows that the $\bar{R}_{sa}$ interaction distance is larger than the critical interaction distance for energy transfer (7.9 Å) only in the film with the lowest manganese concentration, which in turn is in good agreement with its very low $Ce^{3+} \rightarrow Mn^{2+}$ energy transfer efficiency (17.0%).

5. Conclusions

A blue–red emission phosphor excited with ultraviolet radiation can be manufactured with $CeCl_3$-and $MnCl_2$-doped HfO_2 films deposited at 300 °C by the ultrasonic spray pyrolysis technique. The blue emission is due to the 5d → 4f de-excitation of Ce^{3+} ions. The red emission is associated with the $^4T_1(G) \rightarrow {}^6A_1(S)$ de-excitation of Mn^{2+} ions. In addition to the red emission, a green emission band is also observed, mainly at low manganese concentration, which suggests that the Mn^{2+} ions can be located in different environments in the hafnium oxide.

The addition of $MnCl_2$ in the HfO_2:$CeCl_3$ film leads to a nonradiative energy transfer from Ce^{3+} to Mn^{2+} after Ce^{3+} excitation. The nonradiative character of this transfer is inferred from (i) a decrease of the Ce^{3+} overall emission and (ii) an increase in the decay rate of the Ce^{3+} emission, when the Ce3 film is codoped with manganese.

The critical interaction distance between Ce^{3+} and Mn^{2+} ions for energy transfer, assuming an electrical dipole–quadrupole mechanism, is lower than the one estimated assuming a random distribution of Ce^{3+} and Mn^{2+} ions, so that it is likely that the dopant ions tend to form Ce^{3+}–Mn^{2+} clusters in the HfO_2 film. Further, in such clusters the Ce^{3+} ions tend to be closer to the Mn^{2+} ions as the manganese concentration increases.

The efficiency of the $Ce^{3+} \rightarrow Mn^{2+}$ energy transfer, obtained from emission spectra, is enhanced by increasing the Mn^{2+} content, being up to about 78% for the film with the highest manganese concentration (5 at.%). Moreover, in this film (Ce3Mn5) a purer red emission is obtained, which is required for display applications. The energy transfer efficiency higher than 50% achieved by the Ce3Mn3 and Ce3Mn5 films can make the HfO_2:$CeCl_3$:$MnCl_2$ films interesting phosphors for the design of luminescent layers emitting simultaneously in the three primary colors (blue, green and red).

Acknowledgments

This work was supported by the CONACyT under project contract 43016-F. We would like to thank the CBI chemical laboratory of the Universidad Autónoma Metropolitana-Iztapalapa for sharing its equipment. The authors thank L Baños and the technical assistance of M Guerrero, A B Soto and Z Rivera. One of us, RM, gratefully acknowledges the CONACyT for a postdoctoral stay financial support.

References

[1] Blasse G and Grabmaier B C 1994 *Luminescent Materials* (New York: Springer) p 138
[2] Sundqvist J, Harsta A, Aarik J, Kukli K and Aidla A 2003 *Thin Solid Films* **427** 147
[3] Wilk G D, Wallace R M and Anthony J M 2001 *J. Appl. Phys.* **89** 5243
[4] Villanueva-Ibañez M, Le Luyer C, Dujardin C and Mugnier J 2003 *Mater. Sci. Eng.* B **105** 12
[5] Villanueva-Ibañez M, Le Luyer C, Marty O and Mugnier J 2003 *Opt. Mater.* **24** 51
[6] Mattarelli M, Montagna M, Rossi F, Afify N, Bettinelli M, Speghini A, Armellini C, Jestin Y, Rocca F and Gialanella S 2008 *Opt. Mater.* at press
[7] García-Hipólito M, Caldiño U, Alvarez-Fragoso O, Alvarez-Pérez M A, Martínez-Martínez R and Falcony C 2007 *Phys. Status Solidi* a **204** 2355
[8] García-Hipólito M, Alvarez-Fragoso O, Guzmán J, Martínez E and Falcony C 2004 *Phys. Status Solidi* a **201** R127
[9] Falcony C, García M, Ortíz A, Miranda O, Gradilla I, Soto G, Cota-Araiza L, Farias M H and Alonso J C 1994 *J. Electrochem. Soc.* **141** 2860
[10] Caldiño U, Speghini A and Bettinelli M 2006 *J. Phys.: Condens. Matter* **18** 3499
[11] Caldiño G U, de la Cruz C, Muñoz H G and Rubio O J 1989 *Solid State Commun.* **69** 347
[12] Caldiño G U 2003 *J. Phys.: Condens. Matter* **15** 7127
[13] Caldiño G U 2003 *J. Phys.: Condens. Matter* **15** 3821
[14] Di Bartolo B (ed) 1991 *Advances in Nonradiative Processes in Solids* (New York: Plenum) p 282
[15] Kahng D 1968 *Appl. Phys. Lett.* **13** 210
[16] Lira A, Méndez A, Dagdug L, Murrieta S H and Caldiño G U 1999 *Phys. Status Solidi* b **212** 199
[17] Castañeda D, Muñoz H G and Caldiño U 2005 *Opt. Mater.* **27** 1456
[18] Ramírez-Serrano J, Madrigal E, Ramos F and Caldiño G U 1997 *J. Lumin.* **71** 169
[19] Di Bartolo B 1984 *Energy Transfer Processes in Condensed Matter* ed B Di Bartolo (New York: Plenum) p 103
[20] Caldiño U, Hernández-Pozos J L, Flores C, Speghini A and Bettinelli M 2005 *J. Phys.: Condens. Matter* **17** 7297
[21] Martínez-Martínez R, García-Hipólito M, Ramos-Brito F, Hernández-Pozos J L, Caldiño U and Falcony C 2005 *J. Phys.: Condens. Matter* **17** 3647
[22] Langlet M and Joubert J C 1993 *Chemistry of Advanced Materials* ed C N R Rao (Oxford: Blackwell) p 55
[23] Ehrt D 2004 *J. Non-Cryst. Solids* **348** 22
[24] Dexter D L 1953 *J. Chem. Phys.* **21** 836
[25] Blasse G 1969 *Philips Res. Rep.* **24** 131
[26] Aceves R, Caldiño G U, Rubio O J and Camarillo E 1995 *J. Lumin.* **65** 113
[27] Ramos F, Diamant R, Camarillo I, Muñoz H G and Caldiño G U 1996 *J. Mater. Sci. Lett.* **15** 1439
[28] Méndez A, Ramos L F, Riveros H, Camarillo E and Caldiño G U 1999 *J. Mater. Sci. Lett.* **18** 399